REACTION DYNAMICS

Spectroscopic observation of resonances in the F + H_2 reaction

Jongjin B. Kim,[1]* Marissa L. Weichman,[1] Tobias F. Sjolander,[1] Daniel M. Neumark,[1,2]† Jacek Kłos,[3] Millard H. Alexander,[3,4]† David E. Manolopoulos[5]†

Photodetachment spectroscopy of the FH_2^- and FD_2^- anions allows for the direct observation of reactive resonances in the benchmark reaction F + H_2 → HF + H. Using cooled anion precursors and a high-resolution electron spectrometer, we observe several narrow peaks not seen in previous experiments. Theoretical calculations, based on a highly accurate F + H_2 potential energy surface, convincingly assign these peaks to resonances associated with quasibound states in the HF + H and DF + D product arrangements and with a quasibound state in the transition state region of the F + H_2 reaction. The calculations also reveal quasibound states in the reactant arrangement, which have yet to be resolved experimentally.

Much of our understanding of the structures of stable molecules has come from spectroscopy. The analysis of bound-bound transitions yields molecular geometries and frequencies, fingerprints of the molecular potential energy surface (PES). The observation of similar sharp structures during a chemical reaction would give comparable insight into the reactive PES, in particular in the all-important transition state region (*1*). The fleeting nature of the transition state makes this task much more challenging, however. Here, we report the spectroscopic observation of sharp resonance structures associated with the transition state and product valley regions of the F + H_2 → HF + H reaction, a benchmark reaction in the field of chemical reaction dynamics (*2*).

The rapid variation of a scattering cross section with energy or angle has long guided physicists in the investigation of nuclear and subnuclear structure. These so-called resonances are signs of metastable excited states or previously unknown particles. In chemistry, the experimental and theoretical search for these quantum features in reactive scattering experiments has been intense (*3*–*7*). Although tentative experimental evidence for resonances in the F + H_2 reaction was first reported in the 1980s (*8*), it took until 2000 for a resonance to be unambiguously identified in a crossed molecular beam experiment, as a step-like feature in the energy dependence of the integral cross section of F + HD → HF + D (*9*, *10*). The same resonance—a quasibound state in the FHD transition state region with three quanta of excitation in the H–F stretch and none in either the H–D stretch or the bend—has since been found under higher resolution to give rise to undulations in individual state-to-state differential cross sections of the reaction as a function of the collision energy (*11*). More recent molecular beam experiments combined with theoretical simulations have also provided some evidence for a resonance (*12*) [or perhaps two resonances (*13*)] in F + H_2.

Anion photoelectron spectroscopy provides an alternative experimental approach to the study of chemical reactions (*14*). Because the geometry of the FH_2^- anion is close to that of the neutral F + H_2 transition state, photodetachment of the electron from the anion provides a direct spectroscopic probe of the transition state dynamics (*15*), as illustrated in Fig. 1. If the precursor anion is rotationally cold, this probe avoids the averaging over angular momentum that tends to obscure resonances in a crossed molecular beam experiment. Previous spectra of FH_2^- have revealed broad peaks associated with the bending levels of the FH_2 transition state complex, which correspond to the "quantized bottlenecks" of the reaction rather than reactive scattering resonances (*16*). Calculations based on the best potential energy surface then available reproduced the positions and intensities of these broad peaks, as well as predicting a number of narrower peaks, which were assigned to resonances (*17*). Unfortunately, the experimental resolution available at the time (~20 meV) was not high enough to permit the detection of these features.

The development of slow-electron velocity-map imaging (SEVI) with cryogenic ion cooling has enabled the acquisition of photoelectron spectra of complex species with sub–millielectron volt (sub-meV) resolution (*18*). Much improved signal-to-noise ratio compared to that of a previous SEVI report (*19*) has allowed the detection of sharp peaks in the spectra of both FH_2^- and FD_2^-, which we report here.

The experimental apparatus has been described in detail previously (*18*, *20*), with relevant features highlighted in the supplementary materials (*21*). The FH_2^- and FD_2^- ions are created by introducing F^- anions into a cryogenically cooled ion trap containing H_2 or D_2 buffer gas at low pressure; the resulting ion yield is substantially higher than in previous work, where FH_2^- was generated in a molecular beam ion source. The ions are extracted from the trap, mass-selected, and photodetached at various photon energies. The photoelectron kinetic energy (E_{ke}) distribution is obtained with SEVI, in which a velocity-map imaging electron spectrometer (*22*) operated at comparatively low extraction voltages produces high-resolution (sub-meV) photoelectron spectra at low E_{ke}. The electron binding energy (E_{be}) gives the energy difference between the anion and neutral states and is obtained by subtracting the measured E_{ke} from the photon energy. As previous simulations suggested more obvious signatures of resonances with *para*-H_2 than *ortho*-H_2 (*17*), the FH_2^- ions were enriched in *p*-H_2. However, the FD_2^- ions were formed by trapping F^- in a buffer gas of *normal* deuterium (*n*-D_2).

Several earlier publications outline the calculation of the photodetachment spectrum of the FH_2^- anion (*17*, *23*). Photodetachment projects the vibrational wave function of the anion onto the F + H_2 potential energy surface, where it evolves under the influence of the neutral FH_2 Hamiltonian. In the Condon approximation, the photodetachment spectrum $P(E)$ is the Fourier transform of the overlap between this evolving wave function and the initial anion vibrational wave function (*17*). We use here the very high quality LWAL F + H_2 potential energy surface (*24*), which is based on multireference, configuration-interaction calculations. The relation between the experimentally measured binding energy of the electron (E_{be}) and the energy E in the theoretical simulation, which refers to the bottom of the F + H_2 reactant valley with the F atom in its ground ($^2P_{3/2}$) spin-orbit state, is

$$E_{be} = E - ZPE(H_2) + EA(F) + D_0(FH_2^-) \quad (1)$$

where ZPE is the zero-point energy of H_2, EA is the electron affinity of F, and D_0 is the dissociation

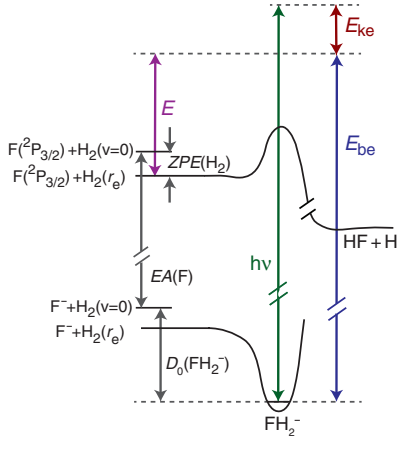

Fig. 1. Schematic of the energetics of the photodetachment process. Arrows show the relationship between the experimental electron binding energy (E_{be}) and the scattering energy (E).

[1]Department of Chemistry, University of California, Berkeley, CA 94720, USA. [2]Chemical Sciences Division, Lawrence Berkeley National Laboratory, Berkeley, CA 94720, USA. [3]Department of Chemistry and Biochemistry, University of Maryland, College Park, MD 20742, USA. [4]Institute for Physical Science and Technology, University of Maryland, College Park, MD 20742, USA. [5]Department of Chemistry, Oxford University, Physical and Theoretical Chemistry Laboratory, South Parks Road, Oxford OX1 3QZ, UK. *Present address: SLAC National Accelerator Laboratory, Menlo Park, CA 94025, USA †Corresponding author. E-mail: dneumark@berkeley.edu (D.M.N.); mha@umd.edu (M.H.A.); david.manolopoulos@chem.ox.ac.uk (D.E.M.)

energy of the FH_2^- anion. These energetics are illustrated schematically in Fig. 1. In the theoretical simulations, we use the experimental *EA* of F [3.4012 eV (*25*)] and the *ZPE*s for H_2 and D_2 as predicted by the LWAL PES (0.2705 and 0.1918 eV, respectively). To determine D_0, we have performed new ab initio and vibrational bound state calculations described in the supplementary materials, obtaining D_0 = 0.2005 eV for FH_2^- and 0.2219 eV for FD_2^-.

The experimental and simulated SEVI spectra of *p*-FH_2^- and *n*-FD_2^- are presented in Figs. 2 and 3, respectively. Spectra at additional photon energies are shown in figs. S1 and S2. Figures S3 and S4 show a comparison of the *p*-FH_2^- photodetachment spectra obtained with two different anion wave functions (fig. S3) and two different potential energy surfaces (fig. S4).

The overview *p*-FH_2^- photodetachment spectrum is dominated by three broad peaks, labeled A, B, and C in Fig. 2. These had been previously assigned to hindered H_2 rotor (or bending) states of the transient FH_2 complex (*16*, *26*). The equilibrium geometry of the linear FH_2^- anion is just on the reactant side of the neutral transition state. Because the minimum F + H_2 barrier on the neutral potential energy surface has a bent geometry, photodetachment of the electron excites a bending progression in the neutral FH_2 complex. We also observe a smaller peak in the high-resolution *p*-FH_2^- spectrum (purple), labeled a, just above the first broad peak A. This peak has not been resolved in any previous experiment. It also occurs in the simulated spectra, along with two smaller peaks (labeled β and γ) at higher energy, and a pronounced peak (labeled α, seen experimentally as a slight shoulder) on the low-energy side of peak A.

The situation for *n*-FD_2^- is similar. The experimental overview spectrum in Fig. 3 is dominated by two broad peaks, labeled D and E. The high-resolution spectrum shows two smaller peaks at lower energy, labeled b and c. These smaller peaks are also seen in the theoretical spectra, along with an additional small peak labeled δ, which is not resolved in the experimental spectrum. In both cases (*p*-FH_2^- and *n*-FD_2^-), the agreement between the positions of the calculated and the observed high-resolution peaks (peak a in Fig. 2 and peaks b and c in Fig. 3) is excellent, suggesting that an analysis of the theoretical calculations will provide a reliable guide to the origin of these experimental peaks. What makes this comparison especially compelling is that no arbitrary shift was introduced to align the experimental and theoretical spectra in Figs. 2 and 3; use of the ab initio values of D_0 for FH_2^- and FD_2^- in the relationship between E and E_{be} in Eq. 1 locates the theoretical spectra.

Calculating the scattering wave function $\psi(E)$ at the energy E of each peak allows us to characterize the peaks in the theoretical spectra in Figs. 2 and 3. This is the same procedure used previously by Russell and Manolopoulos (*17*). The details of the present, more accurate calculations of the wave functions $\psi(E)$ are given in the supplementary materials (*21*).

Figure 4 shows plots of the wave functions corresponding to the low-energy resonance peaks α, A, and a in Fig. 2 and peaks b, c, and δ in Fig. 3, in collinear F–H–H (F–D–D) geometry. This figure unambiguously reveals the nature of the peaks in the photodetachment spectra: Peaks α and δ are reactant resonances, peak A is a transition state resonance, and peaks a, b, and c are product resonances. The quasibound states that give rise to these resonances are localized in the reactant F + H_2 (F + D_2) van der Waals well, the FH_2 transition state, and the product HF + H (DF + D) van der Waals well, respectively. The green contours in Fig. 4 depict the anion wave functions.

It is possible to assign quantum numbers to the resonance wave functions on the basis of their nodal structure. The reactant resonances have quantum numbers v, j, and t, where v enumerates the number of quanta in the H–H stretch; j, in the hindered H_2 rotation; and t, in the F–H_2 stretch of the F + H_2 van der Waals complex. For the product resonances, v', j', and t' refer, similarly, to the H–F stretch, the hindered HF rotation, and the H–HF van der Waals stretch. The quantum numbers of the reactant resonances in Fig. 4 are (v,j,t) = (0,0,0) for both α (*p*-FH_2^-) and δ (*n*-FD_2^-), whereas the quantum numbers of the product resonances are (v',j',t') = (3,0,0)

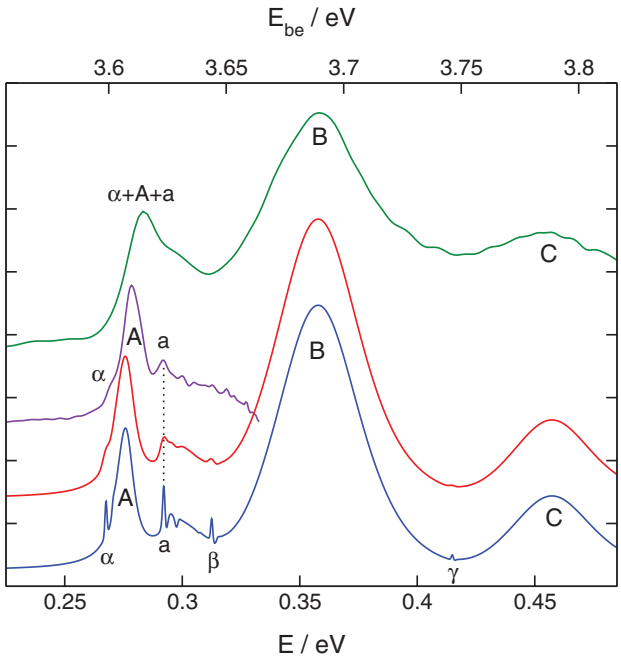

Fig. 2. Photodetachment spectra of *p*-FH_2^-. Green: experimental overview spectrum (~10 meV resolution). Purple: highest-resolution experimental spectrum (2 to 3 meV) over a narrower energy window. Blue: theoretical simulation at 1 meV energy resolution. Red: convolution of the theoretical simulation over a Gaussian function with full width at half maximum (FWHM) of 3 meV. The calculated spectra have not been shifted to match experiment. The relation between the experimental electron binding energy E_{be} and the energy E relative to $F(^2P_{3/2})$ + $H_2(r_e)$ is given by Eq. 1 as $E_{be} = E + 3.3312$ eV.

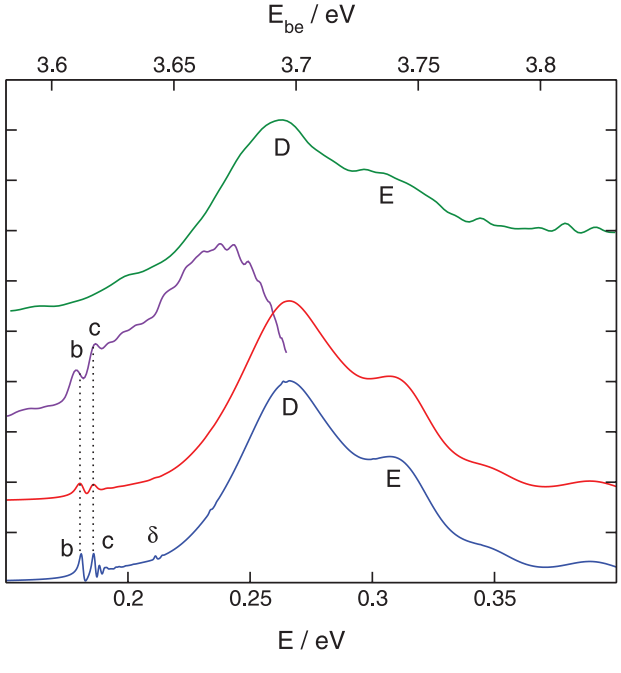

Fig. 3. Photodetachment spectra of *n*-FD_2^-. Green: experimental overview spectrum (~10 meV resolution). Purple: highest-resolution experimental spectrum (2 to 3 meV) over a narrower energy window. Blue: theoretical simulation at 1 meV energy resolution. Red: convolution of the theoretical simulation over a Gaussian function with FWHM of 3 meV. The calculated spectra have not been shifted to match experiment. The relation between the experimental electron binding energy E_{be} and the energy E relative to $F(^2P_{3/2})$ + $H_2(r_e)$ is given by Eq. 1 as E_{be} = E + 3.4313 eV.

for a and (v',j',t') = (4,0,0) and (4,0,1) for b and c, respectively. Finally, the transition state resonance that gives rise to peak A in the p-FH_2^- spectrum has three quanta in the H–F stretch (ν_1) and none in either the F–H–H bend (ν_2) or the H–H stretch (ν_3).

The resonances a, b, and c that have been detected as narrow peaks in the present high-resolution SEVI spectra of p-FH_2^- and n-FD_2^- are thus all product resonances: quasibound states localized in the van der Waals well region in the product valley. For additional clarification, fig. S5 shows how well the positions of the FH–H and FD–D product state resonances are captured by an adiabatic-bender model (*27*–*29*). Because the energies of these resonances are below the thresholds for production of HF(v' = 3) + H and DF(v' = 4) + D, they cannot decay into these channels and must decay instead into HF(v' = 2) + H and DF(v' = 3) + D by vibrational predissociation (the hallmark of a Feshbach resonance). The reason why there are two resonances for FD_2 and only one for FH_2 can be traced to the larger mass of D, which leads to two quasibound states in the D–DF(v' = 4, j' = 0) van der Waals stretching coordinate rather than just one (see the supplementary materials for a more detailed analysis). The emergence of peak a at high resolution was predicted by Russell and Manolopoulos in their earlier theoretical study of the p-FH_2^- spectrum (*17*), but peaks b and c in the n-FD_2^- spectrum have been neither predicted nor measured until now.

The broader low-energy peak A in the p-FH_2^- spectrum was previously assigned to a "direct scattering" or "quantized bottleneck" state associated with the opening of the F + H_2(v = 0, j = 0) channel at the transition state (*17*). However, it is clear from the present calculations that the wave function $\psi(E)$ at the energy of this peak is localized in the transition state region rather than delocalized along the reaction coordinate. This localization is the characteristic feature of a resonance wave function (*30*). This resonance has precisely the same form and quantum numbers as the transition state resonance found by Skodje *et al.* in the F + HD reaction (*9*, *10*). It is thus simply an analytic continuation of this resonance in the mass of one of the two hydrogen atoms. It is the broad peaks B and C in Fig. 2 and D and E in Fig. 3 that are due to quantized bottlenecks, with wave functions that are delocalized along the reaction coordinate (*30*); the associated wave functions are shown in fig. S6.

All of the other peaks in Figs. 2 and 3 can be assigned in the same way by examining the scattering wave functions at the peak energies. The results of these assignments are summarized in Table 1. The narrow peaks β and γ in Fig. 2 are reactant resonances with quantum numbers (v,j,t) = (0,2,0) and (0,4,0), respectively. Like peak δ in Fig. 3, the theoretical calculations predict only low intensity for these peaks. They have yet to be resolved experimentally. As shown in fig. S4, the agreement between the experimental and theoretical resonance positions is noticeably poorer with the use of another recently developed F + H_2 surface (*31*), illustrating that the resonances are indeed a sensitive and experimentally accessible probe of the neutral reactive surface.

We have shown that high-resolution SEVI photodetachment spectra of p-FH_2^- and n-FD_2^- anions reveal previously unresolved peaks in the low-energy region that can unambiguously be attributed to reactive scattering resonances. The signatures of these resonances in the SEVI spectra are far clearer than they would be in a crossed molecular beam experiment, where angular momentum averaging washes out resonance features in both integral and differential cross sections.

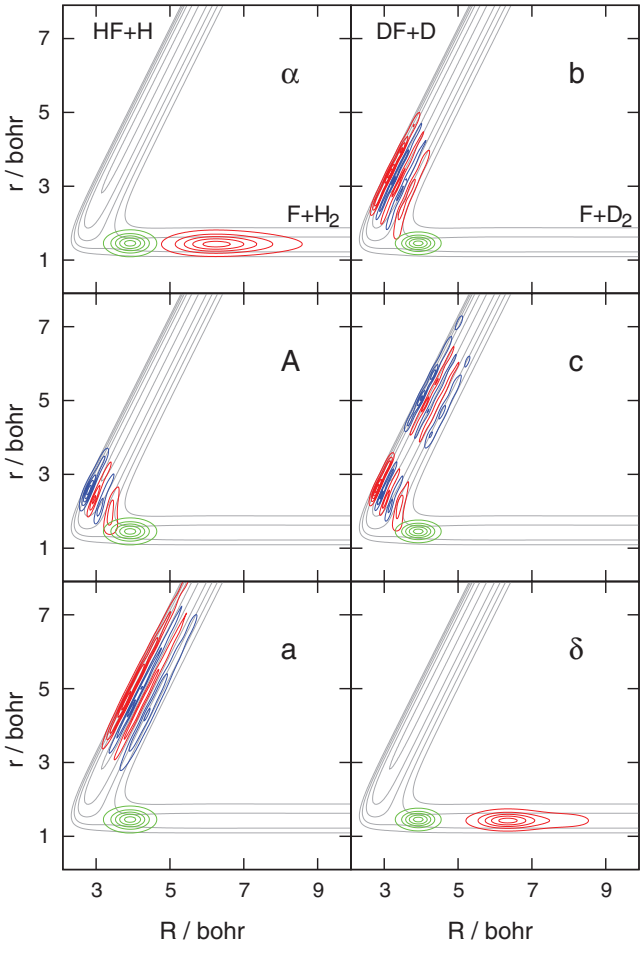

Fig. 4. Resonance wave functions. The wave functions $\psi(E)$ at the energies E of the first three peaks in the p-FH_2^- spectrum in Fig. 2 (α, A, and a; left), and the first three peaks in the n-FD_2^- spectrum in Fig. 3 (b, c, and δ; right), plotted in collinear geometry, as red [$\psi(E) > 0$] and blue [$\psi(E) < 0$] contours, as a function of the distance R between F and the center-of-mass of H_2 (D_2) and the bond length r of H_2 (D_2). Superimposed in gray are contours of the LWAL potential energy surface (*24*). Contours of the FH_2^- and FD_2^- anion wave functions are shown in green for comparison. The contoured regions of all wave functions encompass probability density values greater than 10% of their maxima; the apparent lack of overlap between the anion wave functions and some of the resonance wave functions arises because the overlap is in the tail (<10%) of the probability distribution.

Table 1. Assignment of the peaks in the p-FH_2^- and n-FD_2^- photodetachment spectra in Figs. 2 and 3. The quantum numbers given for the quantized bottlenecks (see fig. S6) are those of the reactant channel that becomes energetically accessible as a hindered rotor (bending) state at the transition state at the energy of the peak in the photodetachment spectrum.

Spectrum	Peak	E/eV	Assignment	Quantum numbers
p-FH_2^-	α	0.2676	Reactant resonance	(v,j,t) = (0,0,0)
	A	0.2758	Transition state resonance	(ν_1,ν_2,ν_3) = (3,0,0)
	a	0.2921	Product resonance	(v',j',t') = (3,0,0)
	β	0.3125	Reactant resonance	(v,j,t) = (0,2,0)
	B	0.3578	Quantized bottleneck	F + H_2(v = 0, j = 2)
	γ	0.4149	Reactant resonance	(v,j,t) = (0,4,0)
	C	0.4573	Quantized bottleneck	F + H_2(v = 0, j = 4)
n-FD_2^-	b	0.1809	Product resonance	(v',j',t') = (4,0,0)
	c	0.1860	Product resonance	(v',j',t') = (4,0,1)
	δ	0.2112	Reactant resonance	(v,j,t) = (0,0,0)
	D	0.2661	Quantized bottleneck	F + D_2(v = 0, j = 2)
	E	0.3071	Quantized bottleneck	F + D_2(v = 0, j = 4)

Thanks to recent experimental developments (including SEVI and, crucially for the present study, the use of a cryogenically cooled ion trap to produce large amounts of p-FH_2^- and n-FD_2^-), high-resolution anion photodetachment spectroscopy does indeed provide an effective way to observe the elusive resonances in F + H_2 reactive scattering, as was predicted by Russell and Manolopoulos almost 20 years ago (*17*).

REFERENCES AND NOTES

1. J. C. Polanyi, A. H. Zewail, *Acc. Chem. Res.* **28**, 119–132 (1995).
2. D. E. Manolopoulos, *J. Chem. Soc. Faraday Trans.* **93**, 673–683 (1997).
3. G. C. Schatz, *Science* **288**, 1599–1600 (2000).
4. F. Fernández-Alonso, R. N. Zare, *Annu. Rev. Phys. Chem.* **53**, 67–99 (2002).
5. X. Yang, D. H. Zhang, *Acc. Chem. Res.* **41**, 981–989 (2008).
6. R. T. Skodje, in *Advances in Quantum Chemistry*, C. A. Nicolaides, E. J. Brändas, R. S. John, Eds. (Academic Press, New York, 2012), vol. 63, pp. 119–163.
7. K. Liu, in *Advances in Chemical Physics*, S. A. Rice, A. R. Dinner, Eds. (Wiley, Hoboken, NJ, 2012), vol. 149, pp. 1–46.
8. D. M. Neumark, A. M. Wodtke, G. N. Robinson, C. C. Hayden, Y. T. Lee, *J. Chem. Phys.* **82**, 3045 (1985).
9. R. T. Skodje *et al.*, *J. Chem. Phys.* **112**, 4536 (2000).
10. R. T. Skodje *et al.*, *Phys. Rev. Lett.* **85**, 1206–1209 (2000).
11. W. Dong *et al.*, *Science* **327**, 1501–1502 (2010).
12. T. Wang *et al.*, *J. Phys. Chem. Lett.* **5**, 3049–3055 (2014).
13. M. Qiu *et al.*, *Science* **311**, 1440–1443 (2006).
14. D. M. Neumark, *Phys. Chem. Chem. Phys.* **7**, 433–442 (2005).
15. I. M. Waller, T. N. Kitsopoulos, D. M. Neumark, *J. Phys. Chem.* **94**, 2240–2242 (1990).
16. D. E. Manolopoulos *et al.*, *Science* **262**, 1852–1855 (1993).
17. C. L. Russell, D. E. Manolopoulos, *Chem. Phys. Lett.* **256**, 465–473 (1996).
18. C. Hock, J. B. Kim, M. L. Weichman, T. I. Yacovitch, D. M. Neumark, *J. Chem. Phys.* **137**, 244201 (2012).
19. T. I. Yacovitch *et al.*, *Faraday Discuss.* **157**, 399–414, (2012).
20. A. Osterwalder, M. J. Nee, J. Zhou, D. M. Neumark, *J. Chem. Phys.* **121**, 6317–6322 (2004).
21. Methods are detailed in the supplementary materials at *Science* Online.
22. A. T. J. B. Eppink, D. H. Parker, *Rev. Sci. Instrum.* **68**, 3477 (1997).
23. J. Z. H. Zhang, W. H. Miller, *J. Chem. Phys.* **92**, 1811 (1990).
24. F. Lique, G. Li, H.-J. Werner, M. H. Alexander, *J. Chem. Phys.* **134**, 231101 (2011).
25. C. Blondel, C. Delsart, F. Goldfarb, *J. Phys. At. Mol. Opt. Phys.* **34**, 2757 (2001).
26. S. E. Bradforth, D. W. Arnold, D. M. Neumark, D. E. Manolopoulos, *J. Chem. Phys.* **99**, 6345 (1993).
27. S. L. Holmgren, M. Waldman, W. Klemperer, *J. Chem. Phys.* **67**, 4414 (1977).
28. M. H. Alexander, S. Gregurick, P. J. Dagdigian, *J. Chem. Phys.* **101**, 2887 (1994).
29. J. F. Castillo, D. E. Manolopoulos, K. Stark, H.-J. Werner, *J. Chem. Phys.* **104**, 6531 (1996).
30. D. E. Manolopoulos, *Nature* **419**, 266–267 (2002).
31. B. Fu, X. Xu, D. H. Zhang, *J. Chem. Phys.* **129**, 011103 (2008).

ACKNOWLEDGMENTS

The experimental part of this work was funded by the Air Force Office of Scientific Research (AFOSR) under grant no. FA9550-12-1-0160 and the Defense University Research Instrumentation Program (DURIP) under grant no. FA9550-11-1-0330. M.L.W. thanks the National Science Foundation for a graduate research fellowship. The experimental data are available upon request from dneumark@berkeley.edu. M.H.A. is grateful for partial support by the U.S. National Science Foundation under grant CHE-1213332. D.E.M. is funded by the Wolfson Foundation and the Royal Society.

SUPPLEMENTARY MATERIALS

www.sciencemag.org/content/349/6247/510/suppl/DC1
Materials and Methods
Supplementary Text
Figs. S1 to S7
Tables S1 and S2
References (*32*–*59*)

4 June 2015; accepted 9 July 2015
10.1126/science.aac6939

BORON CATALYSIS

Metal-free catalytic C-H bond activation and borylation of heteroarenes

Marc-André Légaré, Marc-André Courtemanche, Étienne Rochette, Frédéric-Georges Fontaine*

Transition metal complexes are efficient catalysts for the C-H bond functionalization of heteroarenes to generate useful products for the pharmaceutical and agricultural industries. However, the costly need to remove potentially toxic trace metals from the end products has prompted great interest in developing metal-free catalysts that can mimic metallic systems. We demonstrated that the borane (1-TMP-2-BH_2-C_6H_4)$_2$ (TMP, 2,2,6,6-tetramethylpiperidine) can activate the C-H bonds of heteroarenes and catalyze the borylation of furans, pyrroles, and electron-rich thiophenes. The selectivities complement those observed with most transition metal catalysts reported for this transformation.

Transition metal–catalyzed reactions are ubiquitous tools in the pharmaceutical and agrochemical industries, despite the costs associated with removing residual catalysts; trace metals in products for human consumption are heavily regulated by international bodies (*1*). Similar concerns exist in the modern electronics industry, where metals need to be removed from organic electronic devices to avoid loss of efficiency (*2*). Nevertheless, the importance of selectively forming bonds between carbon and other atoms using transition metals has been acknowledged by three Nobel Prizes in Chemistry in the past 15 years. More recently, the catalytic functionalization of C-H bonds using transition metals has emerged as an atom-economical way to generate new bonds without the need for activated precursors (*3*, *4*). Through such an activation process, the catalytic C_{sp2}-H borylation of aromatic molecules generates organoboronates (*5*–*7*), which are important species for the pharmaceutical industry and in the field of modern organic materials, notably as building blocks for the creation of new bonds using the Suzuki-Miyaura cross-coupling reaction (*8*, *9*). Although some base metal complexes have been used as catalysts for the borylation of arenes (*10*–*12*), the most efficient systems to date rely on noble metals, most notably iridium (*6*, *7*). Alternatively, borenium or boronium species generated by highly reactive precursors can promote the electrophilic borylation of arenes, but stoichiometric quantities of amine derivatives are generally needed to generate the active boron reagents (*13*–*15*).

Noble metals are well suited to cleave aromatic C-H bonds in catalytic processes because they can easily mediate two-electron transfer processes.

Département de Chimie, Centre de Catalyse et Chimie Verte (C3V), Université Laval, 1045 Avenue de la Médecine, Québec, QC G1V 0A6, Canada.
***Corresponding author. E-mail: frederic.fontaine@chm.ulaval.ca**

In the borylation reaction using iridium catalysts, this transformation is usually assisted by the boryl substituents present on the metal center, which

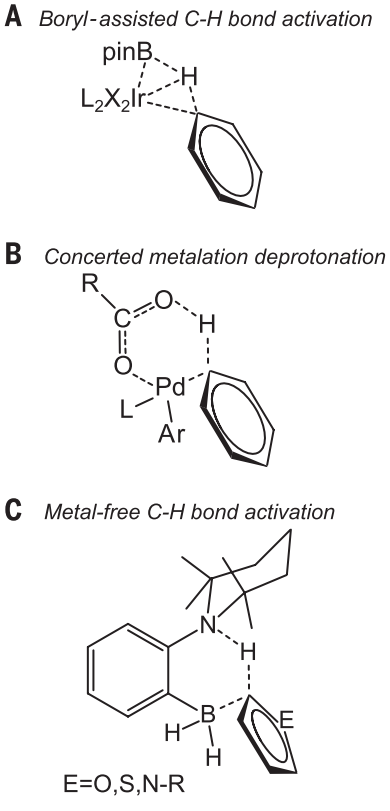

Fig. 1. Representative transition states for the C-H activation of arenes. (**A**) Activation of C-H bonds in borylation transformations using Ir catalysts. (**B**) Carboxylate-assisted metalation deprotonation at palladium. (**C**) Metal-free C-H activation of heteroarenes using FLP catalysts. The dashed lines represent bonds formed and cleaved during the electron transfer.

Spectroscopic observation of resonances in the F + H_2 reaction

Jongjin B. Kim *et al.*

Science **349**, 510 (2015);
DOI: 10.1126/science.aac6939